Effect of solution chemistry on the removal of Co(II) on rice straw-derived biochar

Lijia Dong[a], Wensheng Linghu[b], Donglin Zhao[c], Yinyan Mou[a], Baowei Hu[a,*],
Abdullah M. Asiri[d], Khalid A. Alamry[d], Di Xu[e], Jin Wang[f,*]

[a]*School of Life Sciences, Shaoxing University, Huancheng West Road 508, Shaoxing, Zhejiang, 312000, China,*
emails: hbw@usx.edu.cn (B. Hu), Donglijia@126.com (L. Dong), 315848957@qq.com (Y. Mou)
[b]*School of Chemistry and Chemical Engineering, Shaoxing University, Huancheng West Road 508, Shaoxing, Zhejiang, 312000,*
China, email: wslinghu@usx.edu.cn
[c]*School of Materials and Chemical Engineering, Anhui University of Architecture, Hefei 230601, China, email: 554602303@qq.com*
[d]*Chemistry Department, Faculty of Science, King Abdulaziz University, Jeddah 21589, Saudi Arabia,*
emails: aasiri2@kau.edu.sa (A.M. Asiri), k_alamry@yahoo.com (K.A. Alamry)
[e]*State Key Laboratory of Lake Science and Environment, Nanjing Institute of Geography and Limnology, CAS,*
Nanjing 210008, China, email: dxu@niglas.ac.cn
[f]*College of Environmental Science and Engineering, Guangzhou University, Guangzhou 510006, China,*
email:wangjin200726@hotmail.com

ABSTRACT

Herein, the sorption of Co(II) onto rice straw-derived biochar as a function of various environmental conditions was investigated in batch experiments. The removal efficiency was strongly affected by pH but not by ionic strength over the whole pH range. At low pH values, inner-sphere surface complexation dominated the sorption. While at high pH values, both precipitation and inner-sphere surface complexation controlled sorption process. The kinetics was simulated well by the pseudo-second-order model and was affected by both the film diffusion and the intraparticle diffusion model. The initial Co(II) concentration significantly enhanced the sorption amount of Co(II) on biochar, but weakly affected the sorption rate. Any of the Langmuir, Freundlich, and Dubinin–Radushkevich isotherm models could simulate sorption isotherms well, while the Langmuir model fitted it the best. The thermodynamic data implied the Co(II) sorption was enhanced at high temperature and was a spontaneous and endothermic process. In addition, the biochar can be employed repeatedly in Co(II) sorption process. These results demonstrate that rice straw-derived biochar can be a suitable adsorbent for Co(II) removal from aqueous solutions.

Keywords: Biochar; Co; Sorption; HA/FA; Thermodynamic parameters

1. Introduction

Cobalt, a heavy metal mainly presenting in effluent from nuclear power plants and some other industries, often threatens the health of human and causes various disease [1–3], thereby, various techniques including precipitation, ion-exchange, oxidation, reverse osmosis, membrane electrolysis, and sorption have been used to remove Co(II) from aqueous solutions [4,5]. Among these techniques, sorption is one of the most effective ways on account of its several advantages such as simplicity of the design, cost-efficiency, and widely application [4].

It is a fact that different adsorbents can exhibit different sorption capabilities. For example, the sorption of Co(II) on γ-alumina [6], hydroxyapatite [7], γ-Al_2O_3 [8], magnetic multiwalled carbon nanotube [9], graphene oxides [10], and amination graphene oxide nanocomposite [11]

has been investigated. According to these investigations, it is found that there are some limitations for each above-mentioned adsorbent. For example, the sorption efficiency is not high enough, or the adsorbent is difficult to be separated [4]. Thereby, developing a new adsorbent to overcome these shortcomings is meaningful for the application in future.

Biochar is drawing more and more attention due to its low cost and excellent capacity to remove several heavy metals from aqueous solutions. Compared with other low-cost methods (i.e., sand filtration, boiling, solar disinfection, and chlorination), biochar has two obvious merits in water treatment: (1) biochar is a low-cost and renewable adsorbent produced by readily available biomaterials and skills, making it appropriate for low-income communities; (2) biochar maintains original properties of water, while other methods generate carcinogenic by-products (e.g., chlorination) and/or increase concentrations of chemical contaminants (e.g., boiling) [12]. In addition, biochar is commonly produced from agricultural residues which are waste or by-products from harvesting of crops such as corn, peanut, sorghum, and sugarcane, but are scarcely utilized [13]. Thus, there is dual benefit to utilize these agricultural residues as feedstock for making biochar.

In general, the removal of metal ions from an aqueous solution is dependent on solution pH, ionic strength, solid content, and other parameters. Therefore, it is important to study whether the variance of these parameters affects the removal of metal ions. In this paper, we used the residues of *Oryza sativa* as feedstock to obtain biochar through pyrolysis techniques. The sorption of Co(II) on biochar derived from rice straw was investigated as a function of various solution chemical conditions including contact time, initial concentrations, pH, ionic strength, humic substances, solid content, and temperature. The Co(II) sorption kinetics was simulated by the pseudo-second-order model, the liquid film diffusion model, and the intraparticle diffusion model to illustrate the kinetics interaction mechanism. The sorption isotherms were simulated by the Langmuir, Freundlich, and Dubinin–Radushkevich (D–R) sorption models to determine the interaction mechanism between Co(II) and biochar. Thermodynamics of the sorption process was also investigated to demonstrate the characteristics of Co(II) adsorption on biochar. The novelty of this study is that a kind of agriculture waste (rice straw) is employed as the raw material of an adsorbent for Co(II) removal, which has never been reported and may bring to bi-benefits for environmental protection. This study would be very useful for improving the long-term performance of rice-straw derived biochar in field applications.

2. Experimental

2.1. Materials

The rice straw, a kind of common agricultural residue, was selected as the feedstock of biochar in this experiment. First, we collected the rice straw from Shaoxing city, Zhejiang province, China. Subsequently, the plant residues were air dried, crushed, and ground to < 1.0 mm particle size. Finally, the ground particles were slowly pyrolyzed at 600°C in a pyrolyzer under no supply of air for 2 h. The heating rate was set to 7°C/min. The obtained biochar samples were cooled

to room temperature and stored in desiccators before use. All reagents used in this experiment were analytical reagent grade without further purification.

Humic acid (HA) and fulvic acid (FA) were extracted from the soil in Hua-Jia County (Gansu province, China). HA and FA widely exist in aquatic environments and can complex with heavy metals and interact with adsorbents due to their various functional groups [6,8]. Thereby, HA and FA can strongly influence the sorption efficiency of heavy metal by adsorbents.

2.2. Characterization of biochar

The biochar was characterized by scanning electron microscopy (SEM), transmission electron microscopy (TEM), Fourier-transform infrared (FTIR), the zeta potential, energy dispersive X-ray (EDX) spectroscopy, the average pore diameter, and the specific surface area. SEM and EDX measurements were carried out using a field emission SEM (JSM-6360LV, Japan). The TEM images were obtained using a TEM (JEM-1011, Japan). The FTIR spectroscopy was acquired using a FTIR spectrometer (NEXUS, America) in the range of wavenumber 4,000–400 cm^{-1}. The spectral resolution and the range of energy ratio were set to 2 cm^{-1} and 25%–40%, respectively. The zeta potential of the biochar sample was measured using a zeta potential analyzer (Zetasizer Nano ZS, Malvern Co., UK). Brunauer, Emmett, and Teller (BET) and Barrett, Joyner, and Halenda (BJH) models were employed to measure specific surface area and pore volume of the biochar samples, respectively.

2.3. Batch sorption experiments

Batch techniques were used to test the sorption of Co(II) on biochar derived from rice straw at three temperatures, that is, 293, 313, and 333 K. All experiments were conducted in 15 mL polyethylene centrifuge tubes. The Co(II) stock solutions, $NaNO_3$ solutions, biochar, and Milli-Q water were added to the above-mentioned tubes in order to obtain the desired concentrations of the different constituents. HNO_3 (0.01 M) and NaOH (0.01 M) were employed to adjust the pH values of solutions. The ratio of the amount of biochar to the solution volume (*m*/*V*) was 0.45 g/L. The tubes were agitated on an oscillator for 24 h to achieve sorption equilibrium. After that equilibrium time, the solid and liquid phases were separated by centrifugation at 9,000 rpm for 30 min. The concentration of Co(II) in the supernatant was analyzed by a spectrophotometer (V-1800, Mapada, Shanghai) at the wavelength of 592 nm using Co(II)-Xylenol orange and hexadecyl trimethyl ammonium bromide.

The Co(II) removal efficiency by biochar [Co(II) sorption (%) = $(C_0 - C_e)/C_0 \times 100$], distribution coefficient [$K_d = (C_0 - C_e)/C_e \times V/m$], and sorption amount onto biochar [$q_e = (C_0 - C_e) \times V/m$] were calculated from the initial Co(II) concentration (C_0, mg/L), the final or equilibrium Co(II) concentration (C_e, mg/L), the biochar mass adsorbed on biochar (*m*, g), and the suspension volume (*V*, L).

To ensure the experimental repeatability and improve data accuracy, all the experimental data were subjected to the averages of duplicate or triplicate experiments. The relative errors of data were less than 5%.

3. Results and discussion

3.1. Characterization of biochar

Fig. 1 shows the SEM image, TEM image, FTIR spectrum, Zeta potentials, and EDX of the biochar samples. The SEM image (Fig. 1(a)) indicates biochar is composited by different size of blocky structures randomly piling up. In more microscopic view (Fig. 1(b)), the structure of biochar is loose and porous. These characteristics may endow the biochar with strong sportive capability. The functional groups on the biochar are examined by the FTIR spectroscopy, as shown in Fig. 1(c). The band at 3,446 cm^{-1} may arise from the O–H stretching vibration [14,15]. The peaks at 1,385 and 1,037 are assigned to carboxyl O=C–O and alkoxy C–O stretching vibrations, respectively [16]. The bands at 794, 519, and 468 may be subjected to the integrated crystalline structure of biochar [17], which needs to be further investigated using the XAFS technique. The zeta potential of the biochar sample as a function of medium pH indicates that the point of pH$_{pzc}$ was ~5.25 (Fig. 1(d)). It can be seen that the biochar samples are positively-charged at low pH values, which is unfavorable for adsorbing cationic Co^{2+} due to electrostatic repulsion, while the biochar samples are negatively-charged at high pH values, which is favorable for adsorbing Co^{2+} due to electrostatic attraction [11].

In addition, the EDX result suggests that the biochar sample contains some nontarget elements (Ca, Si, Mg, Fe, and Al) (Fig. 1(e)). However, compared with the elemental distribution percentage of C atom (84.11%) and O atom (13.81%), the percentage of other nontarget atoms is far lower (2.18%). The result indicates that the rice straw-derived biochar used here contains negligible impurities. In other words, the effects of these impurities on the sorption are considered to be negligible. Finally, by analyzing the BJH pore-size distribution and corresponding TN2 adsorption-desorption isotherms, we find the average pore diameter and the specific surface area of the biochar is 45.43 nm and 61.11 m^2/g, respectively.

3.2. Effect of contact time and initial cobalt concentration

The sorption of Co(II) on biochar derived from rice straw with different initial concentrations as a function of time is shown in Fig. 2(a). It is obvious that Co(II) is rapidly adsorbed on biochar during the initial 1.5 h of contact time, and then the sorption becomes slow until reaching equilibrium. The high sorption rate may be attributed to a large number of available sites at the beginning of the reaction, but as the sites are gradually filled, the sorption becomes slow [18]. Fig. 2(a) also shows that the percent of Co(II) removal increases with the increase of the initial Co(II) concentrations. In general, the initial Co(II) concentration can provide driving force to overcome the resistance to the mass transfer of Co(II) ions onto biochar, thereby the increase of driving force of the concentration gradient can enhance Co(II) sorption [19]. However, the effect of initial Co(II) concentrations on its sorption rate is weak or negligible, indicating that the sorption rate of Co(II) onto biochar over the initial concentration range of 8–12 mg/L is similar. Totally, the similar but rapid sorption processes with different Co(II) concentrations suggest that Co(II) sorption dominates by the chemical sorption or the

surface complexation [4]. The Co(II) concentration strongly enhances the amount of Co(II) sorption, while shows weak effects on the sorption velocity.

In order to simulate the sorption kinetics of Co(II), the pseudo-second-order model, the liquid film diffusion model, and the intraparticle diffusion model are applied to fit the experiment data. The linear form of the pseudo-second-order model, liquid film diffusion model, and intraparticle diffusion can be expressed as [19–22]:

$$\frac{t}{q_t} = \frac{1}{2Kq_e^2} + \frac{t}{q_e} \tag{1}$$

$$\ln\left(1 - \frac{q_t}{q_e}\right) = -K_t \tag{2}$$

$$q_t = k_i t^{0.5} \tag{3}$$

where q_t represents the Co(II) sorption amount (mol/g) at t (h) time; k (g/(mol h)) is the rate constant. K_i [mol/(g·h$^{1/2}$)] is the diffusion rate. As shown in Fig. 2(b), all the linear relationships between t/q_t and time (t) with three different Co(II) concentrations are significant (Table 1, $P < 0.001$) and the correlation coefficients are close to 1, suggesting that the uptake kinetics of Co(II) follow the pseudo-second-order rate equation.

The Co(II) sorption onto biochar may comply with the three processes: film diffusion process, particle diffusion process, and chemical reaction process (see the details for the paper written by Mckay and Poots [23]). Among the three processes, the film or particle diffusion process may control the sorption and is the rate-limited step, while chemical reaction process is rapid and can be negligible [23]. The rate-limited film diffusion process and particle diffusion process can be modeled by the liquid film diffusion model and the intraparticle diffusion model, respectively.

It is well-known that the sorption kinetics is controlled by the film diffusion process if the plot of $-\ln(1-q_t/q_e)$ versus t yields a line with zero intercept. In Fig. 2(c), the intercept of the three lines is not found to be zero, which indicates that the film diffusion process is not the single rate-limiting step in the Co(II) sorption. For the intraparticle diffusion model (Fig. 2(d), Table 1), one can see that the plots do not pass the origin, implying that the intraparticle diffusion process is also not the only rate control step although this step may strongly affect Co(II) sorption process. From the results, it is concluded that the kinetic sorption is not dominated by the liquid film diffusion or intraparticle diffusion model solely.

3.3. Effect of pH and ionic strength

The pH value of solutions can change functional groups on the adsorbent surface and the species of an adsorbate, and thus pH can affect the sorption process [24]. The sorption of Co(II) on biochar as a function of pH in 0.001, 0.01, and 0.1 M NaNO$_3$ solutions is shown in Fig. 3(a). It is obvious that the sorption is strongly dependent on pH at pH < 9.2 and the Co(II) sorption percentage increases with increasing pH.
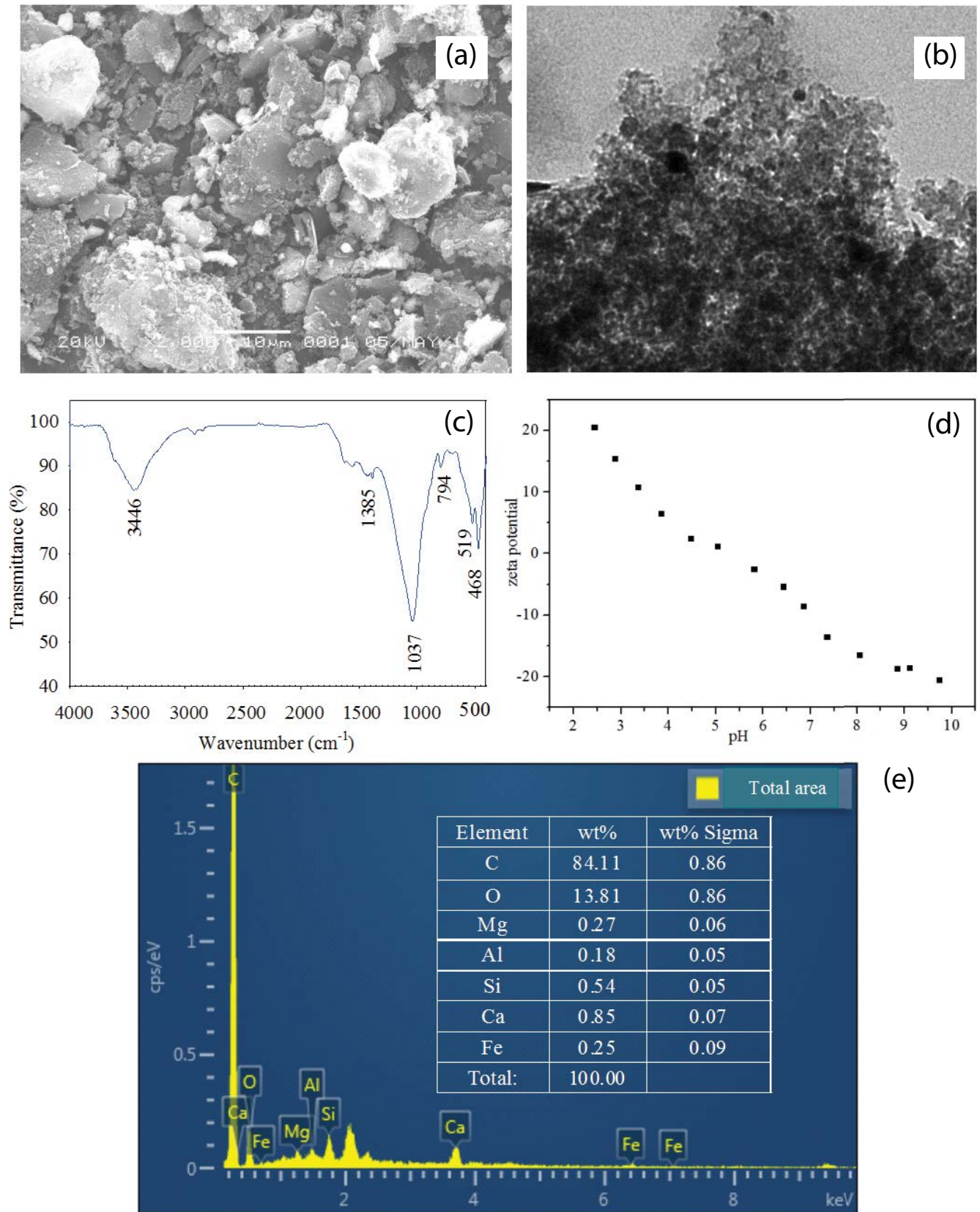
Fig. 1. SEM image (a), TEM image (b), FTIR spectra (c), the zeta potential (d), and EDX(e) of biochar derived from rice straw.
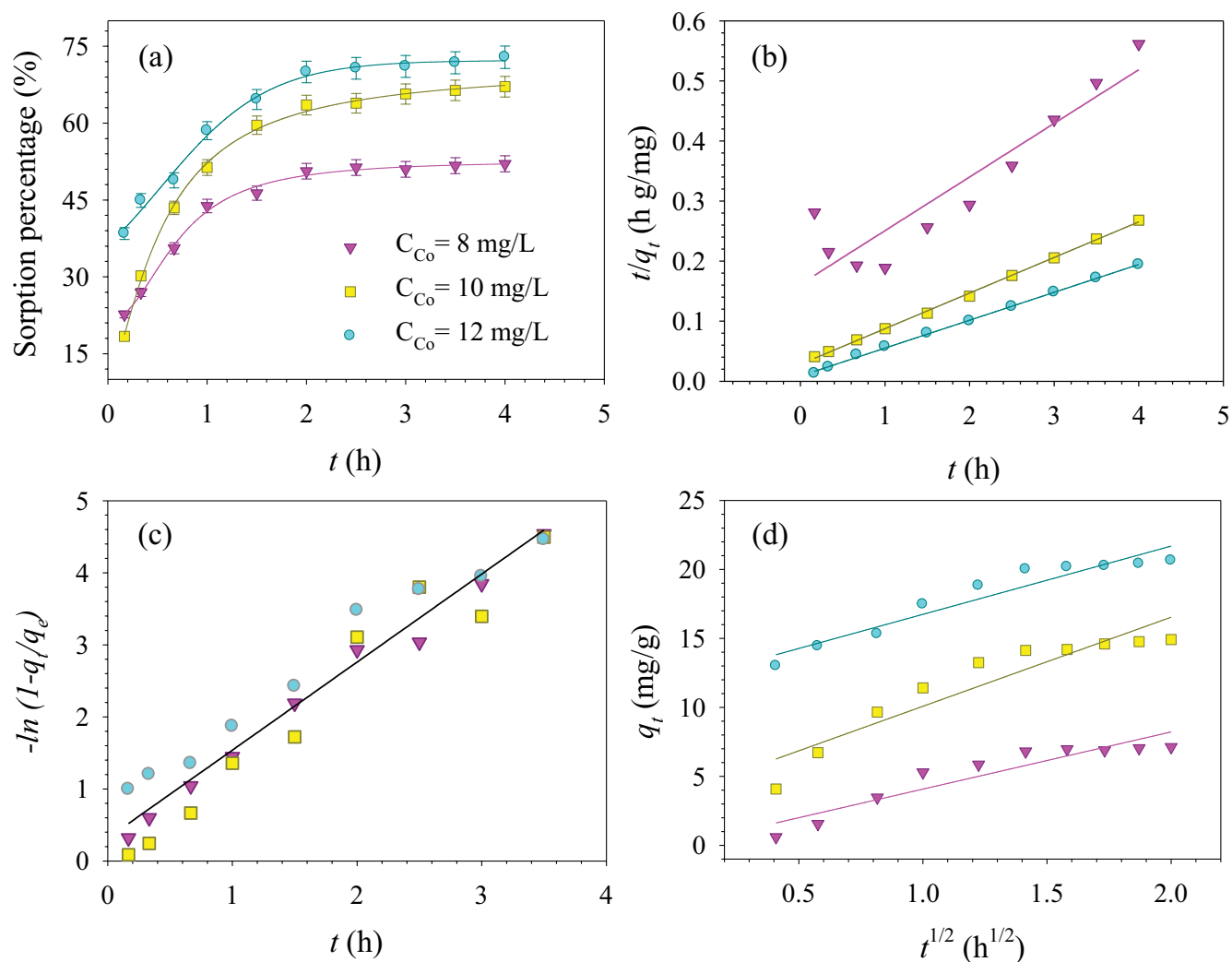
Fig. 2. Effect of contact time on Co(II) sorption percentage with different initial Co(II) concentrations (a); Effect of contact time on the Co(II) sorption amount (b); Plot of t/q_t versus t for the pseudo-second-order model simulation (c); Plot of q_t versus $t^{1/2}$ for the intraparticle diffusion model simulation (d). T = 293 ± 2 K, pH = 6.0 ± 0.2, I (NaNO$_3$) = 0.1 mol/L, and m/V = 0.45 g/L.

Table 1
Kinetic parameters for Co(II) adsorption on biochar derived from rice straw with three different initial Co(II) concentrations (8, 10, and 12 mg/L). T = 293 ± 2 K, pH = 6.0 ± 0.2, I (NaNO$_3$) = 0.1 mol/L, and m/V = 0.45 g/L

Initial concentrations (mg/L)	Pseudo-second-order model			Intraparticle diffusion model	
	q_e (mg/g)	K [g/(mg h)]	R^2	k_{int} [mg/(g h$^{1/2}$)]	R^2
8	11.199	0.0494	0.862	4.145	0.873
10	16.878	0.124	0.999	6.456	0.877
12	21.547	0.245	0.999	4.948	0.921

It is interesting that the sorption curve at different pH can be divided three stages. Specifically, with 10 mg/L cobalt concentration, the Co(II) sorption on biochar slowly increases at the pH range from 2 to 5, then abruptly increases at pH 5–7, and finally, slowly increases until maintaining the high level at pH > 7. At pH > 9.2, approximately 95% of Co(II) has been adsorbed on biochar.

The effect of ionic strength on Co(II) sorption onto biochar was investigated. As illustrated in Fig. 3(a), the effect of ionic strength in a wide pH range is fairly negligible. According to the ionic strength-independence and the pH-dependence of Co(II) sorption, it is concluded that inner-sphere complexes are formed on the surfaces of biochar. Because the ionic strength can alter the thickness and interface potential
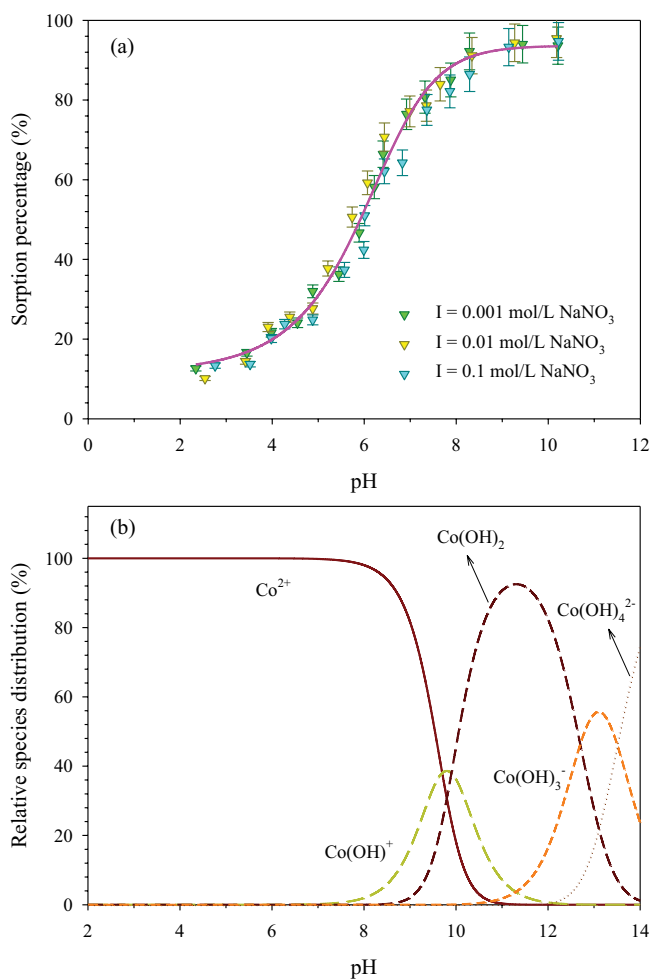
Fig. 3. Effect of pH and ionic strength on Co(II) sorption on the biochar surface (a) and the 3D plot of q_e versus C_e with different pH values (b). T = 293 ± 2 K, $C_{Co(II)initial}$ = 10 mg/L, and m/V = 0.45 g/L.

of the double layer, resulting in the binding of the adsorbing species; the background electrolyte ions are placed in the same plane as the outer-sphere complexes; thereby, outer-sphere surface complexes are deemed to be more susceptible to ionic-strength variations than inner-sphere surface complexes [4,25]. Consequently, Co(II) sorption on biochar is attributed to inner-sphere surface complexation rather than ion exchange or outer-sphere surface complexation.

However, the formation of precipitation is also an important factor affecting the sorption of heavy metals. In aqueous solutions, the relative species of cobalt exist in the forms of Co^{2+}, $Co(OH)^+$, $Co(OH)_2$, $Co(OH)_3^-$, and $Co(OH)_4^{2-}$ at different pH values (Fig. 3(b)). At pH < 7, Co^{2+} is the dominant species. Due to the protonation reaction on biochar surfaces, the concentration of protonated sites decreases. Thus, the sorption efficiency of Co^{2+} decreases as a result of the electrostatic repulsion. However, at pH > 7, the concentration of deprotonated sites increases arising from the surface deprotonation reaction. The deprotonated sites are more available to retain the metal ions, and surface complexation between Co^{2+} and biochar is facilitated, thus resulting in the high

sorption of Co(II). At pH > 8.2, Co^{2+} and $Co(OH)^+$ are the dominant species in solutions, and $Co(OH)_2$ precipitation begins to form, which is the reason why the sorption percentage increases a little [4]. Therefore, the sorption mechanism of Co(II) is inner-sphere surface complexation at low pH values (pH < 8.2), while the removal of Co(II) from aqueous solutions is accomplished by both precipitation and inner-sphere surface complexation at high pH values (pH > 8.2).

3.4. Effect of solid content

The effect of solid content on Co(II) sorption percentage and amount on biochar is shown in Fig. 4. The sorption percentage of Co(II) significantly increases from 20% to 70% with an increase of solid content from 0.1 to 1.0 g/L. The tendency is reasonable because the total numbers of functional sites increase with increasing solid content. Note that the sorption efficiency of biochar toward Co(II) keeps unchanged at m/V > 0.8 g/L. In consideration of reducing the cost of decontamination Co(II), the appropriate content of biochar to remove Co(II) at pH 6.0 is 0.8 g/L. The Co(II) sorption amount in Fig. 4 decreases with rising solid content. This phenomenon may arise from the competition among the colloids of biochar. Because such competition gives rise to the reducing of total specific surface area of biochar and the increasing of the diffusion path length of biochar, which further reduces the effective sites of functional groups on the surface of biochar [4,26,27]. At last, the increasing solid content leads to the decrease of the sorption and complexation ability of biochar toward Co(II).

3.5. Effect of humic substances

Humic substances can strongly complex multivalent elements and consequently change the sorption of these elements on adsorbents due to the high functionality of the humic substances [8]. Herein, the effect of pH on of Co(II) sorption onto biochar in the absence and presence of HA/FA is shown in Fig. 5. The presence of HA/FA enhances Co(II) sorption on biochar at pH < 7.0, while inhibits the sorption at pH > 7.0. Also, there is no gap of the sorption between in the presence of HA and FA in the whole pH range. Similar results are found in many other researches, including Co(II) sorption on γ-alumina [6], Co(II) sorption on γ-Al_2O_3 [8], Eu(III) on graphene oxide [16], U(VI) sorption on NKF-6 zeolite [17], and so on. These findings suggest that the effects of humic substances on the sorption of heavy metals over the whole pH range may be attributed to similar mechanisms. At the low pH values, it is easy to attract the negatively charged HA/FA on the positively charged biochar due to stronger complexation ability between HA/FA and biochar compared with the ability between HA/FA and Co(II). Subsequently, the electrostatic properties of the solid-aqueous interface are modified by HA/FA adsorbed on biochar surface, which finally provides more favorable environment for Co(II) sorption [28]. However, at the high pH values, the solubility of FA/HA increases and the charge on biochar surface becomes negative, which makes the negatively-charged HA/FA difficult to be adsorbed on the surface of biochar. Besides, a part of free stable FA/HA – Co(II) complexes are formed in solutions. Therefore, the sorption of Co(II) on biochar significantly decreases at high pH values.
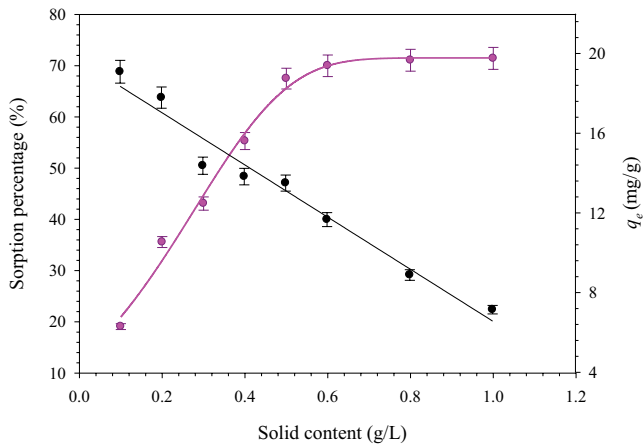
Fig. 4. Effect of solid content on the Co(II) sorption percentage (a) and the 3D plot of q_e versus C_e with different solid contents (b). pH = 6.0 ± 0.2, T = 293 ± 2 K, $C_{Co(II)initial}$ = 10 mg/L, and I (NaNO$_3$) = 0.1 mol/L.
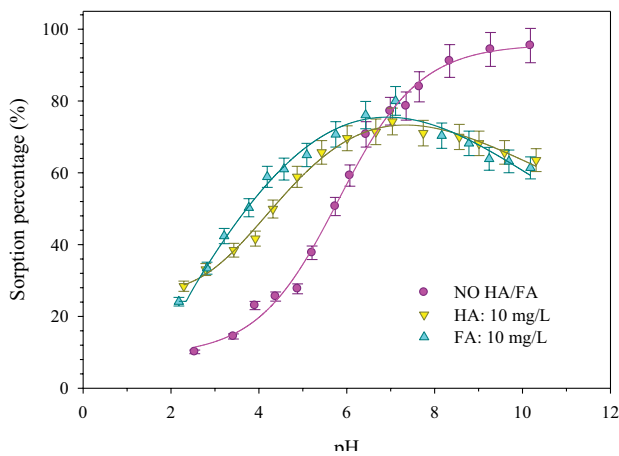
Fig. 5. Effect of HA/FA on Co(II) sorption on biochar derived from rice straw. pH = 6.0 ± 0.2, T = 293 ± 2 K, $C_{Co(II)initial}$ = 10 mg/L, I (NaNO$_3$) = 0.1 mol/L, and m/V = 0.45 g/L.

3.6. Adsorption isotherms and thermodynamic study

The sorption isotherms of Co(II) on biochar at 293, 313, and 333 K are shown in Fig. 6. The Co(II) sorption amount is the lowest at 293 K and highest at 313 K (Fig. 6(a)), suggesting that high temperature enhances the sorption of Co(II) on biochar. To elucidate the sorption capacity of Co(II) ions onto biochar, the equilibrium experimental data were used to simulate the Langmuir, Freundlich, and D–R isotherm equations (Fig. 6(b)–(d)). The Langmuir model generally describes the monolayer sorption process occurring on a homogeneous surface [29]. While the Freundlich model describes the sorption occurring on heterogeneous surface and the sites have different energy of sorption [30]. The D–R model assumes that the traits of the sorption curves are related to the porosity of the adsorbent [31]. The linear forms of the three isotherm models can be expressed as follows [29–31]:

$$\frac{C_e}{q_e} = \frac{1}{K_L q_{max}} + \frac{C_e}{q_{max}} \tag{4}$$

$$\log q_e = \log k_F + n \log C_e \tag{5}$$

$$\ln q_e = \ln q_{max} - \beta \varepsilon^2 \tag{6}$$

where q_{max} (mol/g) and K_L (L/mol) are the Co(II) maximum sorption capacity on per weight unit of biochar and the Langmuir affinity parameter, respectively; K_F [(mol^{1-n} L^n)/g] and n represent the Freundlich affinity-capacity parameter and exponent, respectively; β is the D–R activity constant and ε is the Polanyi potential, which is calculated by RT ln(1 + 1/C_e); From the D–R model, the bonding energy of the ion-exchange mechanism (E, kJ/g) is calculated by $(2\beta)^{-1/2}$. Here, it needs to be noted that R is the universal gas constant (8.314 J/(K mol)), T (K) is the absolute temperature. All the constants calculated from the three models are shown in Table 2.

According to the simulated curves (Fig. 6) and the isotherm constants listed in Table 2, it is obvious that the sorption isotherms can be fit very well by all the three isotherm models. Especially for the Langmuir model, its regression correlation coefficients (R^2) are higher than ones in the other two models, suggesting that the Langmuir model can fit the isotherm best. The better fit of the Langmuir model suggests the Co(II) sorption takes place on homogeneous surface and the sorption process belongs to monolayer sorption [29]. In addition, the values of q_{max} derived from the Langmuir model increase with an increase of temperature, which reveals high temperature is beneficial to Co(II) sorption on biochar. In the Freundlich model, n values are less than 1, which indicates that Co(II) is favorably adsorbed on biochar. Also, the n value becomes lower with increasing temperature, indicating that the sorption intensity becomes stronger at a higher temperature [32]. In the D–R model, the removal of Co(II) can be well explained ($R^2 > 0.970$), but the q_{max} values are different from the q_{max} values in Langmuir model. This discrepancy may be due to the different assumptions between the two models.

Here, the maximum sorption capacity of rice straw-derived biochar fitted by the Langmuir model was compared with the ones of some other materials (Table 3). The biochar shows higher q_{max} value than a series of materials including Fe$_3$O$_4$/bentonite composite [33], magnetite/GO composite [4], and diatomite [34], while has lower q_{max} value than SAC [35], nanocryptomelane [36], and GOs [37]. The result implies that the sorption capacity of rice straw-derived biochar needs to be improved. However, two outstanding merits are subject to the biochar compared with the other three adsorbents. The first one is that the feedstock is easily available. The second one is to solve the problem of environmental pollution from agriculture in China. Thus, the rice straw-derived biochar deserves being further decorated to improve its sorption capacity.

Thermodynamic investigations for Co(II) sorption on biochar at three different temperatures are undertaken to the involved mechanisms. Different thermodynamic parameters such as change in Gibbs free energy (ΔG^0), and entropy (ΔS^0), enthalpy (ΔH^0) are estimated by following equations [38,39]:

$$\Delta G^0 = -RT \ln K^0 \tag{7}$$
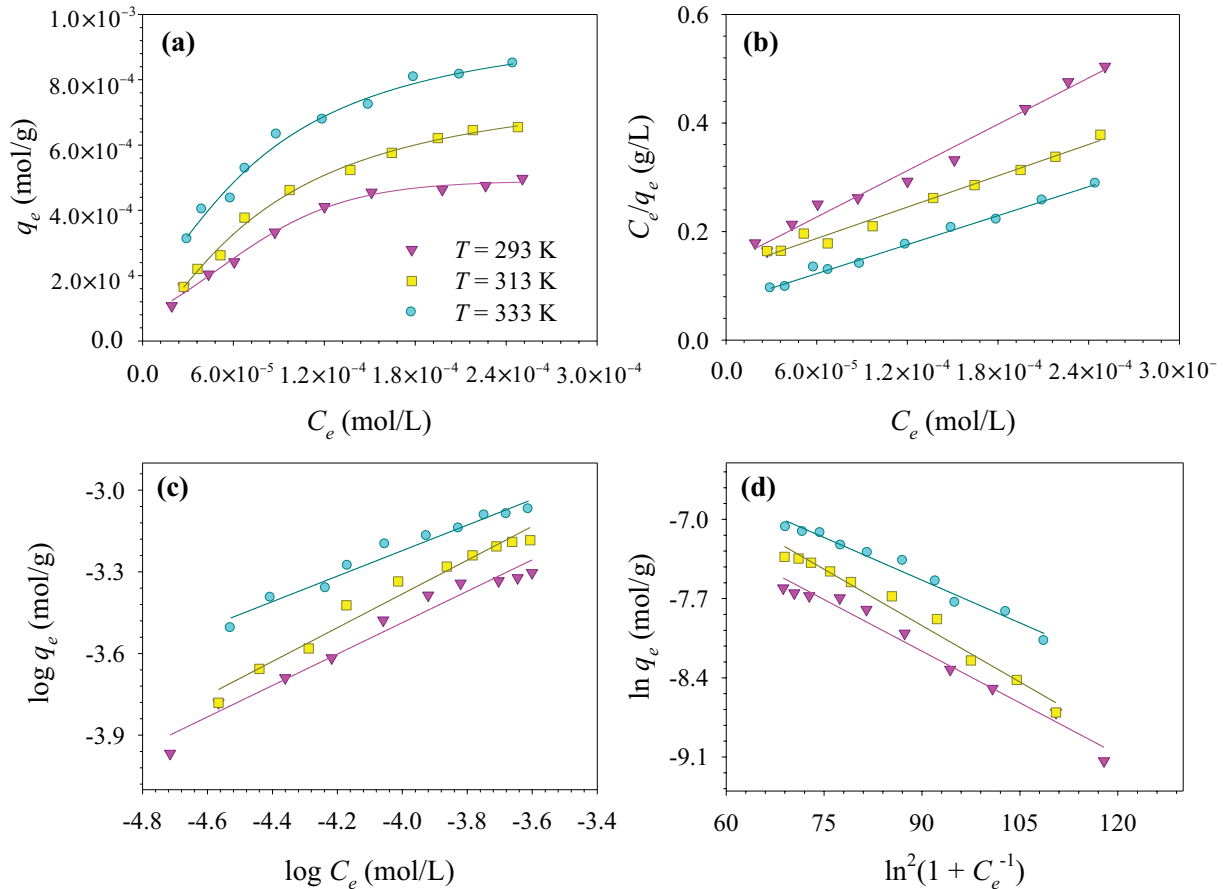
Fig. 6. Sorption isotherm (a), linearized Langmuir isotherm (b), linearized Freundlich isotherm (c), and linearized Dubinin–Radush-kevich isotherm (d) on Co(II) sorption for biochar derived from rice straw at 293, 313, and 333 K. pH = 6.0 ± 0.2, I (NaNO$_3$) = 0.1 mol/L, and m/V = 0.45 g/L.

Table 2
The parameters derived from Langmuir, Freundlich, and D–R isotherms for Co(II) sorption on biochar at three temperatures (293, 313, and 333 K). pH = 6.0 ± 0.2, $C_{Co(II)initial}$ = 10 mg/L, I (NaNO3) = 0.1 mol/L, and m/V = 0.45 g/L

T (K)	Langmuir model		
	q_{max} (mol/g)	b (L/mol)	R^2
293	7.022×10^{-4}	1.009×10^4	0.9837
313	1.039×10^{-3}	7.431×10^3	0.9828
333	1.123×10^{-3}	1.293×10^4	0.9918
T (K)	Freundlich model		
	K_F [(mol^{1-n} L^n)/g]	n	R^2
293	0.0663	0.5770	0.9656
313	0.1259	0.6203	0.9689
333	0.0449	0.4686	0.9654
T (K)	D–R model		
	q_{max} (mol/g)	β	R^2
293	4.397×10^{-3}	0.0304	0.9749
313	7.087×10^{-3}	0.0332	0.9772
333	5.128×10^{-3}	0.0252	0.9727

$$\ln\left(K^0\right) = \Delta S^0/R - \Delta H^0/RT \tag{8}$$

where K^0 represents the equilibrium constant of the sorption reaction, and the values of ln K^0 are obtained by plotting ln K_d versus C_e (Fig. 7(a)). ΔS^0 and ΔH^0 are calculated from the slope and intercept of the plot ln K^0 versus $1/T$ (Fig. 7(b)), respectively. The various thermodynamic parameters at the three temperatures are given in Table 4.

The value of ΔH^0 is positive, indicating the endothermic sorption of Co(II) on biochar. In generally, the process of ions of heavy metals attaching to the surface of adsorbents is exothermic. But the hydration sheath of partial Co(II) ions in the sorption is easier to be destroyed. This process requires energy. Because the endothermicity of the desolation process exceeds that of the enthalpy of adsorption, the final sorption is endothermic. The value of ΔG^0 is negative and becomes more negative with increasing temperature, which suggests that the sorption process is spontaneous and enhanced by higher temperature. A positive value of ΔS^0 reflects partial structure changes of Co(II) and the biochar during the sorption process, leading to an increase of the disorderness at the biochar-solution interface. These results demonstrate that the Co(II) sorption on rice straw-derived biochar is a spontaneous and endothermic process.

Table 3
Adsorption comparison of rice-straw derived biochar and several reported materials for Co(II)

Materials	Experimental conditions	q_{max} (mg/g)	References
Fe_3O_4/bentonite composite	pH 8.0, T 293 K	18.76	[33]
Magnetite/GO composite	pH 6.8, T 343 K	22.70	[4]
Diatomite	pH 6.0, T 333 K	45.00	[34]
Rice-straw derived biochar	pH 6.0, T 333 K	66.26	This work
SAC	pH 6.0; T 303 K	153.85	[35]
Nanocryptomelane	pH 5.6; T 303K	179.6	[36]
GOs	pH 6.8; T 303 K	198.23	[37]

SAC, sulphurised activated carbon; GOs, graphene oxides.
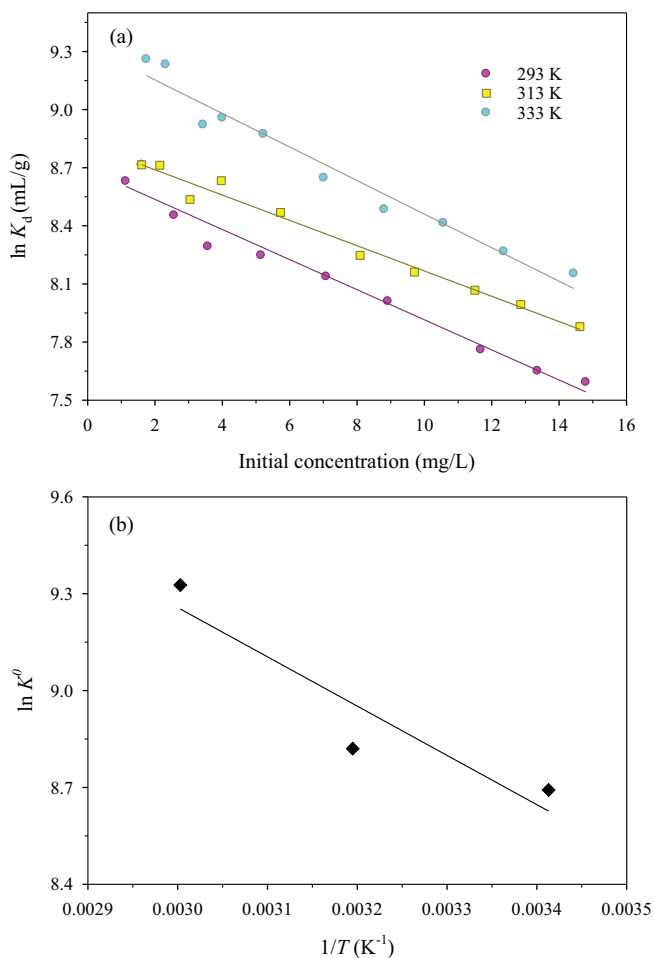
Fig. 7. The linear plots of ln K_d versus C_e for Co(II) sorption at three temperatures (a) and ln K^0 versus $1/T$ (b). pH = 6.0 ± 0.2, I (NaNO$_3$) = 0.1 mol/L, and m/V = 0.45 g/L.

Table 4
The thermodynamic parameters for the sorption of Co(II) on biochar at three temperatures (293, 313, and 333 K). pH = 6.0 ± 0.2, $C_{Co(II)initial}$ = 10 mg/L, I (NaNO$_3$) = 0.1 mol/L, and m/V = 0.45 g/L

T (K)	ΔG^0 (KJ/mg)	ΔS^0 [J/(mg·K)]	ΔH^0 (KJ/mg)
293	−21.174	115.066	12.541
313	−22.952		13.064
333	−25.822		12.495
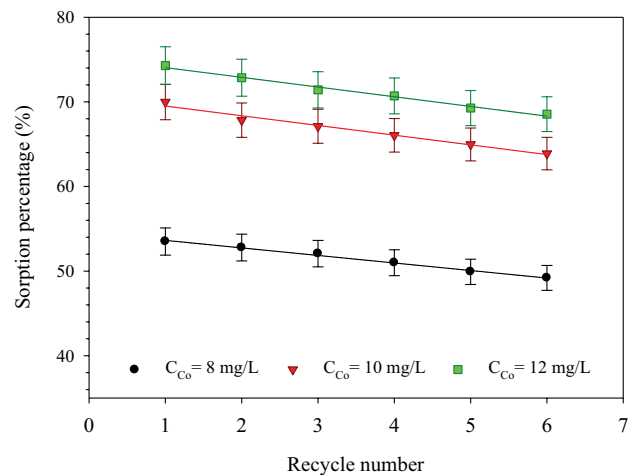
Fig. 8. Recycling of biochar derived from rice straw in the removal of Co(II) from aqueous solutions. pH = 6.0 ± 0.2, T = 293 ± 2 K, I (NaNO$_3$) = 0.1 mol/L, and m/V = 0.45 g/L.

3.7. Desorption and regeneration studies

The estimation on desorption and regeneration properties of rice straw-derived biochar is very important for the application in the removal of heavy metal ions from aqueous solutions [40]. In this research, the biochar was treated with 1.0 M HNO$_3$ to desorb Co(II) from biochar, and then rinsed with Milli-Q water. In the recycling experiments of biochar, the contact time of 5 h was employed in the recovery of Co(III) and the results are shown in Fig. 8. From the results, the sorption percentage of Co(II) on biochar after six circles with 8 mg/L initial Co(II) concentration declined from 54% to 48%. Similar results are found at 10, 12 mg/L initial Co(II) concentrations. The reuse results suggest that the biochar can be employed repeatedly in Co(II) sorption process. And the rice straw-derived biochar possesses a large application perspective for cost-effective removal of Co(II) from aqueous solutions.

4. Conclusions

In this work, the sorption behavior of Co(II) on rice straw-derived biochar was investigated by batch experiments

as a function of various environmental conditions. Co(II) sorption on biochar was rapidly to achieve equilibrium within 2 h and the kinetic sorption could be well simulated by the pseudo-second-order model. Both the film diffusion process and the intraparticle diffusion process affected the sorption kinetics of Co(II) on biochar. Although the initial Co(II) concentration obviously enhanced the sorption amount of Co(II) on biochar, weakly affected the sorption rate. Co(II) sorption on biochar was independent on ionic strength over the whole pH range. The removal of Co(II) was mainly dominated by the inner-sphere complexation at low pH values, but codominated by inner-sphere complexation and precipitation at high pH values. The equilibrium isotherm data indicated that the Langmuir model fitted to the present system better than the Freundlich and D–R models. The thermodynamic results suggested that Co(II) sorption on biochar was a spontaneous and endothermic process, and also enhanced at high temperature. The desorption process indicated that the rice straw-derived biochar can be employed repeatedly in Co(II) sorption process. These results suggest that rice straw-derived biochar can be effectively applied for Co(II) removal from aqueous solution.

Acknowledgments

References

[1] V.D.M. Manohar, B.F. Noeline, T.S. Anirudhan, Adsorption performance of Al- pillared bentonite clay for the removal of cobalt (II) from aqueous phase, Appl. Clay Sci., 31 (2006) 194–206.

[2] V.P. Kudesia, Water Pollution, Pregati Prakashan Publications, Meerut, 1990.

[3] A. Ahmadpour, M. Tahmasbi, T.R. Bastami, J.A. Besharati, Rapid removal of cobalt ion from aqueous solutions by almond green hull, J. Hazard. Mater., 166 (2009) 925–930.

[4] M. Liu, C. Chen, J. Hu, X. Wu, X. Wang, Synthesis of magnetite/graphene oxide composite and application for cobalt(II) removal, J. Phys. Chem. C, 115 (2011) 25234–25240.

[5] V.K. Gupta, I. Ali, Adsorbents for Water Treatment: Development of Low-Cost Alternatives to Carbon Encyclopedia of Surface and Colloid Science, 2nd ed., Taylor & Francis, New York, 2006, pp. 149–184.

[6] S. Yu, X. Li, A. Ren, D. Shao, C. Chen, X. Wang, Sorption of Co(II) on γ-alumina in the presence and absence of fulvic acid, J. Radioanal. Nucl. Chem., 268 (2006) 387–392.

[7] I. Smičiklas, S. Dimović, I. Plećaš, M. Mitrić, Removal of Co^{2+} from aqueous solutions by hydroxyapatite, Water Res., 40 (2006) 2267–2274.

[8] C. Chen, D. Xu, X. Tan, X. Wang, Sorption behavior of Co(II) on γ-Al_2O_3 in the presence of humic acid, J. Radioanal. Nucl. Chem., 273 (2007) 227–233.

[9] Q. Wang, J. Li, C.L. Chen, X.M. Ren, J. Hu, X.K. Wang, Removal of cobalt from aqueous solution by magnetic multiwalled carbon nanotube/iron oxide composites, Chem. Eng. J., 174 (2011) 126–133.

[10] C.W. Song, J. Hu, Y.G. Zhao, D.D. Shao, J.X. Li, Efficient removal of cobalt from aqueous solution using b-cyclodextrin modified graphene oxide, RSC Adv., 3 (2013) 9514–9521.

[11] F. Fang, L.T. Kong, J.R. Huang, S.B. Wu, K.S. Zhang, X.L. Wang, Removal of cobalt ions from aqueous solution by an amination graphene oxide nanocomposite, J. Hazard. Mater., 270 (2014) 1–10.

[12] W. Gwenzi, N. Chaukura, C. Noubactep, F.N.D. Mukome, Biochar-based water treatment systems as a potential low-cost and sustainable technology for clean water provision, J. Environ. Manage., 197 (2017) 732–749.

[13] M.I. Inyang, B. Gao, Y. Yao, Y. Xue, A. Zimmerman, A. Mosa, P. Pullammanappallil, Y. Sik Ok, X. Cao, A review of biochar at a low-cost adsorbent for aqueous heavy metal removal, Crit. Rev. Environ. Sci. Tech., 46 (2015) 406–433.

[14] X.J. Tong, J.Y. Li, J.H. Yuan, R.K. Xu, Adsorption of Cu(II) by biochars generated from three crop straws, Chem. Eng. J., 172 (2011) 828–834.

[15] D. Kołodyńska, J. Krukowska, P. Thomas, Comparison of sorption and desorption studies of heavy metal ions from biochar and commercial active carbon, Chem. Eng. J., 307 (2017) 353–363.

[16] B. Hu, Q. Hu, X. Li, H. Pan, X. Tang, C. Chen, C. Huang, Rapid and highly efficient removal of Eu(III) from aqueous solutions using graphene oxide, J. Mol. Liq., 229 (2017) 6–14.

[17] P. Zong, H. Wang, H. Pan, Y. Zhao, C. He, Application of NKF-6 zeolite for the removal of U(VI) from aqueous solution, J. Radioanal. Nucl. Chem., 295 (2013) 1969–1979.

[18] G.D. Sheng, S.T. Yang, Y.M. Li, X. Gao, Y.Y. Huang, J. Hu, X.K. Wang, Retention mechanisms and microstructure of Eu(III) on manganese dioxide studied by batch and high resolution EXAFS technique, Radiochim. Acta, 102 (2014) 155–167.

[19] Y. Ho, Review of second-order models for adsorption systems, J. Hazard. Mater., 37 (2006) 681–689.

[20] Y. Ho, G. McKay, Pseudo-second order model for sorption processes, Process Biochem., 34 (1999) 451–465.

[21] W.J. Weber, J.C. Morris, Kinetics of adsorption of carbon from solutions, J. Sanit. Eng. Div. Am. Soc. Civ. Eng., 89 (1963) 31–63.

[22] B. Tanhaei, A. Ayati, M. Lahtinen, M. Sillanpää, Preparation and characterization of a novel chitosan/Al_2O_3/magnetite nanoparticles composite adsorbent for kinetic, thermodynamic and isotherm studies of Methyl Orange adsorption, Chem. Eng. J., 259 (2015) 1–10.

[23] G. Mckay, V.J.P. Poots, Kinetics and diffusion-process in color removal from effluent suing wood as an adsorbent, J. Chem. Technol. Biotechnol., 30 (1980) 279–292.

[24] Y. Chen, W. Zhang, S. Yang, A. Hobiny, A. Alsaedi, X. Wang, Understanding of the sorption mechanism of Ni(II) on graphene oxides by batch experiments and density functional theory studies, Sci. China Chem., 4 (2016) 412–419.

[25] K.F. Hayes, J.O. Leclie, Modeling ionic strength effect on cation adsorption at hydrous oxide/solution interfaces, J. Colloid. Interface Sci., 115 (1987) 564–572.

[26] J. Huang, Y. Liu, X. Wang, Selective sorption of tannin from flavonoids by organically modified attapulgite clay, J. Hazard. Mater., 160 (2008) 382–387.

[27] S.T. Yang, D.L. Zhao, H. Zhang, S.S. Lu, L. Chen, X.J. Yu, Impact of environmental conditions on the sorption behavior of Pb(II) in Na-bentonite suspensions, J. Hazard. Mater., 183 (2010) 632–640.

[28] T. Strathmann, S. Myneni, Effect of soil fulvic acid on nickel(II) sorption and bonding at the aqueous-boehmite (γ-AlOOH) interface, Environ. Sci. Technol., 39 (2005) 4027–4034.

[29] I. Langmuir, The adsorption of gases on plane surfaces of glass, mica and platinum, J. Am. Chem. Soc., 40 (1918) 1361–1403.

[30] H.M.F. Freundlich, Uber die adsorption in losugen, J. Phys. Chem., 57 (1906) 385–470.

[31] M.M. Dubinin, The potential theory of adsorption of gases and vapors for adsorbents with energetically non-uniform surfaces, Chem. Rev., 60 (1960) 931–937.

[32] S. Chakraborty, S. Chowdhury, P.D. Saha, Adsorption of crystal violet from aqueous solution onto NaOH-modified rice husk, Carbohydr. Polym., 86 (2011) 1533–1541.

[33] S. Hashemian, H. Saffari, S. Ragabion, Adsorption of cobalt(II) from aqueous solutions by Fe_3O_4/Bentonite nanocomposite, Water Air Soil Poll., 226 (2015) 2212.

[34] G. Sheng, H. Dong, Y. Li, Characterization of diatomite and its application for the retention of radiocobalt: role of environmental parameters, J. Environ. Radioact., 113 (2012) 108–115.

[35] K.A. Krishnan, T.S. Anirudhan, Kinetic and equilibrium modelling of cobalt(II) adsorption onto bagasse pith based sulphurised activated carbon, Chem. Eng. J., 137 (2008) 257–264.

[36] M. Ghaly, E.A. EI-Sherief, S.S. Metwally, E.A. Saad, Utilization of nano-cryptomelane for the removal of cobalt, cesium and lead ions from multicomponent system: kinetic and equilibrium studies, J. Hazard. Mater., 352 (2018) 1–16.

[37] X. Liu, Y. Huang, S. Duan, Y. Wang, J. Li, Y. Chen, T. Hayat, X. Wang, Graphene oxides with different oxidation degrees for Co(II) ion population management, Chem. Eng. J., 302 (2016) 763–772.

[38] R.K. Gautam, A. Mudhoo, M.C. Chattopadhyaya, Kinetic, equilibrium, thermodynamic studies and spectroscopic analysis of Alizarin Red S removal by mustard husk, J. Environ. Chem. Eng., 1 (2013) 1283–1291.

[39] V.K. Gupta, C.K. Jain, I. Ali, M. Sharma, V.K. Saini, Removal of Cadmium and nickel from wastewater using bagasse fly ash-a sugar industry waste, Water Res., 37 (2003) 4038–4044.

[40] J. Wang, Z. Chen, W. Chen, Y. Li, Y. Wu, J. Hu, A. Alsaedi, N.S. Alharbi, J. Dong, W. Linghu, Effect of pH, ionic strength, humic substances and temperature on the sorption of Th(IV) onto NKF-6 zeolite, J. Radioanal. Nucl. Chem., 310 (2016) 597–609.